CHEMISTRY OF MATERIALS

pubs.acs.org/cm

Article

Design of Experiments for Optimization of Polyoxometalate Syntheses

Nicola L. Bell,[†] Manuel Kupper,[†] and Leroy Cronin*

Cite This: *Chem. Mater.* 2021, 33, 7263–7271

Read Online

ACCESS | Metrics & More | Article Recommendations | Supporting Information

ABSTRACT: Design of experiments (DOE) is a key method for optimizing physical processes by altering multiple variables at once to assess their effect. In chemistry, DOE explores a wider parameter space than the dominant "One Factor at a Time" (OFAT) method providing greater opportunity to explore the factors that can be used to optimize yield, purity, and to explore chemical space for new compounds. One area of chemistry that suffers from low yields and poor reproducibility but is full of hard to predict and interesting materials is polyoxometalate cluster science. Herein, we developed a DOE analysis methodology to explore the parameter space of polyoxometalate cluster formation to explore the subtle input effects that are known to have an impact on the product discovery, purity, and stability under the preparation conditions. Using a Plackett–Burman screening design, we analyzed the effect of six synthetic parameters in only 12 experiments, following up with a full factorial analysis of the three most significant factors to identify the key parameters in the successful synthesis of each. Based on this, we provide a useful template that produces the input data for automated synthesis based on DOE on other synthetic procedures. In our POM test cases, redox agent stoichiometry was found in three of the four systems studied to be significant factors with pH and temperature, which also found to be commonly important. The insights derived from this analysis were applied to design optimized synthetic procedures and improve the yield of the product by on average >33% from the highest reported literature yield. Thus, the DOE methodology outlined here is shown to yield insights into reaction optimization rapidly with facile experimental design and analysis even for complex multivariate synthetic procedures.

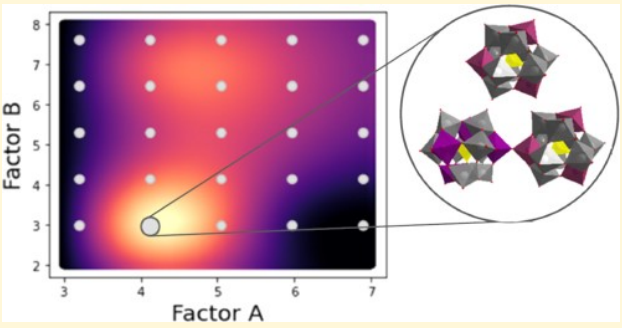

With increasing automation of chemistry allowing the execution of massively parallel reaction process optimization, the exploration of chemical space faces a combinatorial explosion of reaction possibilities. As such the identification of noninnocent factors (i.e., those which change the process outcome) is vital as is exploring multidimensional chemical space in the most resource efficient and productive manner. Chemists have long utilized intuition-led OFAT methods for the catalyst and process optimization despite the fact that it is has been largely discredited.[1] Of the many limitations of OFAT methods perhaps the most relevant to chemistry are that it is highly dependent upon the starting point in chemical space,[2] can result in different labs reaching different scientific conclusions about the impact of the same factors, and is subject to stochastic responses if, as is common, each data point is only collected once.

Design of experiments (DOE) is a branch of applied statistics that provides a more robust and comprehensive search of the chemical space in question from fewer experiments than required for OFAT methods.[3] The method was developed initially for use in agriculture by Ronald A. Fisher in the 1920s and 1930s. Since then, it has become a powerful tool in engineering,[4] administration, pharmaceuticals,[5,6] the food industry,[7,8] energy,[9] and chromatography[10] as well as being applicable to physical processes and computer simulation models.[11] The principle of DOE is to arrange input variables or factors (e.g., temperature, stoichiometry, etc.) in such a way that their effects on a measured response (e.g., yield, purity) can be calculated relatively easily but robustly. In contrast to the dominant one factor at a time (OFAT) methodology where each parameter is varied individually, DOE is designed to provide the maximum information from the least number of experiments, by changing multiple factors at the same time such that a larger experimental space can be explored and a "global" optimum can be found (Figure 1).[12] The method takes into account the fact that the response may be nonlinear in multidimensional experimental space. DOE also has the ability to unravel combinations of multiple main

Received: April 27, 2021
Revised: August 12, 2021
Published: September 14, 2021

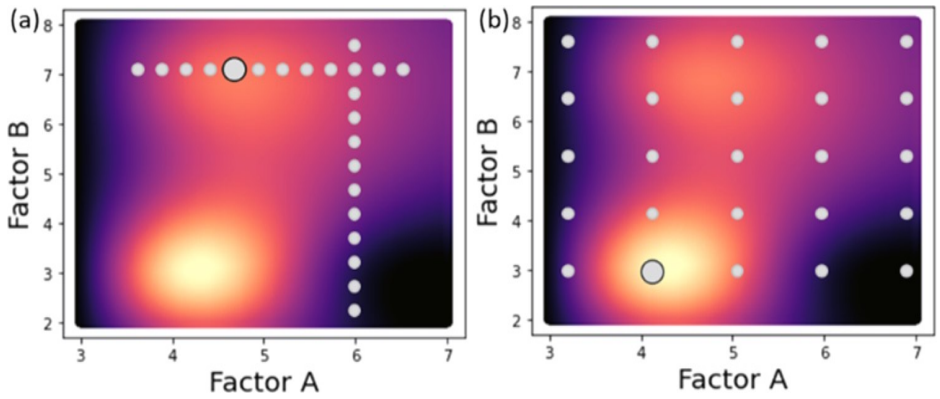

Figure 1. Experimental space can be explored using (a) one factor at a time (OFAT) or (b) design of experiment (DOE) methods. The latter covers the space more efficiently and is more likely to find the global optimum in multidimensional space.

factors working together, so-called factor interactions,[13] which could have a substantial impact on the outcome of a reaction and stay undetected using traditional OFAT methods. Instead, using DOE, it is possible to not only unravel all factors that are significant to the desired outcome (i.e., yield) but also uncover the important interactions that may deliver a deeper understanding of the synthesis and potentially the mechanism of formation for a desired target.

Plackett–Burman designs (PB, Figure 2) are one type of DOE design that can be used to examine syntheses with large

Factors / Runs	A e.g. Conc.	B e.g. Temp.	...	K Dummy 5	Y [%]
1	1	1	...	-1	Y_1
2	1	-1	...	1	Y_2
3	-1	1	...	1	Y_3
...	...	...	...	...	...
12	-1	-1	...	-1	Y_{12}
Σ{Y(-1)}	0.2	21	...	1.1	
Σ{Y(+1)}	3.8	0.6	...	8.3	
Effect	0.6	-3.4	...	1.2	

Figure 2. Example of a Plackett–Burman screening design with 12 runs (11 factor, two level). Factors to be varied: A–F, responses: y_n (i.e., yield), factor settings: −1 (low)/+1 (high). Negative effect values indicate higher yield at the low setting, while positive effects represent increased yield at the higher setting. The absolute value of the effect indicates the magnitude of the impact on yield.

numbers of reaction steps without performing all of the experiments required for a full analysis. A PB design can examine up to $(n - 1)$ factors in n experiments, where n is a multiple of 4, ergo a design with 12 experiments can examine up to 11 factors.[14] A two-level plan allows each factor to have either a low (−1) or a higher value (+1), and each run is undertaken with the various factors set at different levels. The design is completed with dummy factors if the number of examined factors is smaller than $(n - 1)$. The effects of these imaginary factors can be used in statistical analysis of the main effects.[15] Such methods that allow the variation of a large number of factors can be advantageous to exploratory work by revealing the significant factors of a complex synthetic process, where little is known about the key formation parameters making it ideal for highly sensitive and/or unreliable syntheses such as in polyoxometalate (POM) chemistry.

POM chemistry is an attractive and dynamic field covering fundamental and applied research, synthesis and reactivity, physiochemistry and biochemistry, and many other domains.[16] These polyatomic ions occur as molecular metal oxide clusters of transition metals (e.g., Mo, W, V, etc.) in their high oxidation state linked together by shared oxygen atoms. Due to the self-assembly nature of their formation, their syntheses can be very sensitive with the slightest deviation in the process able to influence the success of a reaction. This may be partly because many of the key parameters of POM synthesis are known to interact with each other. For example, variation of the solution pH strongly influences the reduction potential of the metal center and olation behavior changing the effect of the reducing agent added or stirring time in an aerobic environment. The mechanics of many clusters' and materials' formations are still relatively unclear, although recent studies suggest a subtle autocatalytic effect for some POMs.[17] Therefore, many POMs that have been reported are later found to be extremely challenging to reproduce or provide products with very low yields.

In the light of these issues, we have utilized DOE to investigate the following four candidate reactions of large polyoxometalate structures to improve yields and gain insights into the formation mechanism: The Keggin network with the molecular formula $(C_4H_{10}NO)_n[W_{72}Mn_{12}O_{268}Si_7]$ (Figure 3), the $\{V_{18}\}$ network $[Fe_3V_{18}O_{42}(H_2O)_{12}(XO_4)]$ (X = V, S) (Figure 4), the $\{Mo_{154}\}$ blue wheel $Na_{14}[Mo_{154}O_{462}H_{14}(H_2O)_{70}]$ (Figure 6), and the $\{Mo_{132}\}$ brown Keplerate $(NH_4)_{42}[Mo_{132}O_{372}(CH_3COO)_{30}(H_2O)_{72}]$ (Figure 7).

METHODOLOGY

For all syntheses, a 12-run, two-level Plackett–Burman design was chosen as an initial screening method as this allows us to determine the significant main factors by performing substantially fewer than the 64 reactions, which would be required for a full analysis.[18] Several repetitions of each set were carried out, especially when responses varied considerably, to make sure the results were reliable and comparable by their averages. To neutralize any uncontrolled inputs and to control for blocking effects, the running order within the 12 runs was randomly determined for all setups by rolling a dodecahedral die and running them in two different blocks on

https://doi.org/10.1021/acs.chemmater.1c01401
Chem. Mater. 2021, 33, 7263–7271

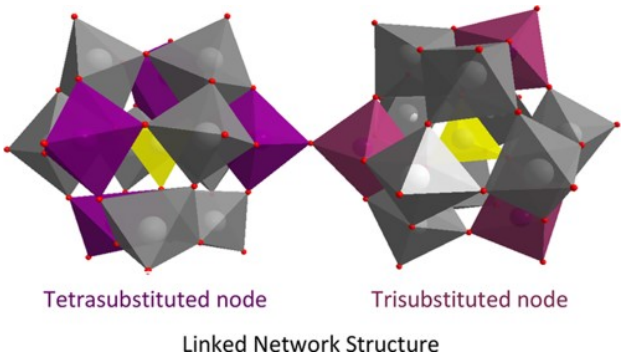

Figure 3. Keggin network is built from two types of lacunary Keggin clusters, which act as either trigonal (mauve) or tetrahedral nodes (purple). The polyhedral representation of the clusters shows the two different secondary building units (SBUs) that are linked into an infinite 3D framework based upon bridging oxo's connecting the clusters.

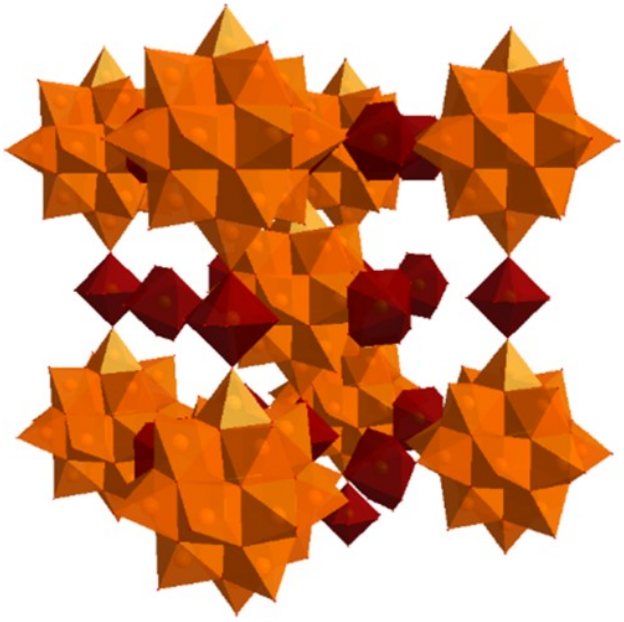

Figure 4. Polyhedral and ball and stick representation of the cubic arrangement of the $\{V_{18}\}$ network linked through Fe^{II} centers, where the $\{VO_5\}$ polyhedra = cyan and Fe = dark red.

different days. Each repeat of the 12-run design was carried out in a different randomly assigned running order. Each step of the procedure was assigned to a factor column (controlled inputs A–F) in the design table, and the high levels (+1) and low levels (−1) were defined. The five remaining columns were assigned to dummy factors (G–K). Usually, three dummy factors are sufficient to calculate the experimental error later; however, more can easily be used, if fewer main factors than possible are investigated in the design.[19]

The original values of each reported experimental step were taken as a starting point, and the factorial levels were set by either adding 10% or deducting 10% of the original values for most of the factors. The design matrix in the following Figure 2 was elaborated and used as a template for all experiments (see the SI, Table S1). A setup was generated that had all solid reagents added as stock solutions and used DrySyn Blocks to distribute the heat equally to all reactors. Total volumes were kept the same within all experiments by adding deionized water. Afterward, the minimum significant factor effects were calculated from the experimental error using the effects of the dummy factors and the corresponding *t*-value of 1.476 based on the degrees of freedom, which was 5 in this case (i.e., the number of Dummy Factors) and the statistical significance level of 20% (i.e., $\alpha = 0.2$).

Before being able to compare the effects with each other they had to be disentangled because the more the number of experiments is reduced using the Plackett–Burman screening method the more main factors and two-factor interactions influence one another, which means that their effects are confounded (see the SI). Higher-order interactions, such as three or more factor interactions, could be neglected in screening due to the hierarchy ordering principle.[20]

The disentangled effects could then be calculated from eq 1.

$$\text{effect (factor)} = \frac{2 \times [\sum (y+) - (y-)]}{n} \quad (1)$$

where $y+$ is the yield when the factor in question is at the higher setting and $y-$ is the yield when the factor is at the lower setting (n = number of factors). If the disentangled factor effect was positive, the product yield increased at the factors maximum setting, and if it was negative, the product yield increased at the factors minimum setting. While every reagent, solvent or other experimental parameter plays a role in the syntheses, only a few were considered as significant to the outcome of the reaction. This so-called sparsity-of-effect principle presumes that the total number of factor effects that dominate the system is small.[20] Accordingly, the three main factors with the largest individual effect on the yield of the desired POM were then analyzed for two-factor interactions using a three-factor full factorial design. This involves multiplying the values for the two factors in question (i.e., A and B) and calculating the effect of the new column (AB). All main and two-factor interactions were then rated based on their overall effect on product yield and purity (determined by ICP).

RESULTS AND DISCUSSION

Keggin Network. The so-called "Keggin-Net" belongs to a class of porous materials with an open three-dimensional structure and can be formulated as $(C_4H_{10}NO)_n[W_{72}Mn_{12}O_{268}Si_7]\cdot zH_2O$. It was first reported in 2008[21] and is the first example of a mesoporous POM-based framework, where the scaffold consists exclusively of transition metal-substituted polyoxometalates (TMSP). This means it is based solely on α-Keggin clusters $[\alpha\text{-}XM_zW_{12-z}O_{40}]^{n-}$ with two different substitution modes ergo two distinct building blocks (Figure 3). Importantly, they are connected to each other directly in the absence of any external electrophilic linkers. The distribution of Mn-substituted addenda is crucial to the framework because both tetrahedral and trigonal-linked building blocks must be present. The morpholinium cations serve as counterions to stabilize the anionic framework and are added at the beginning of the synthesis so potentially have a templating effect. They are embedded in large cavities in the crystal structure formed by rings of 10 Keggin clusters accompanied by two more secondary building units (SBU) on each side and may be important for crystallization as without them the framework might stay soluble.

https://doi.org/10.1021/acs.chemmater.1c01401
Chem. Mater. 2021, 33, 7263–7271

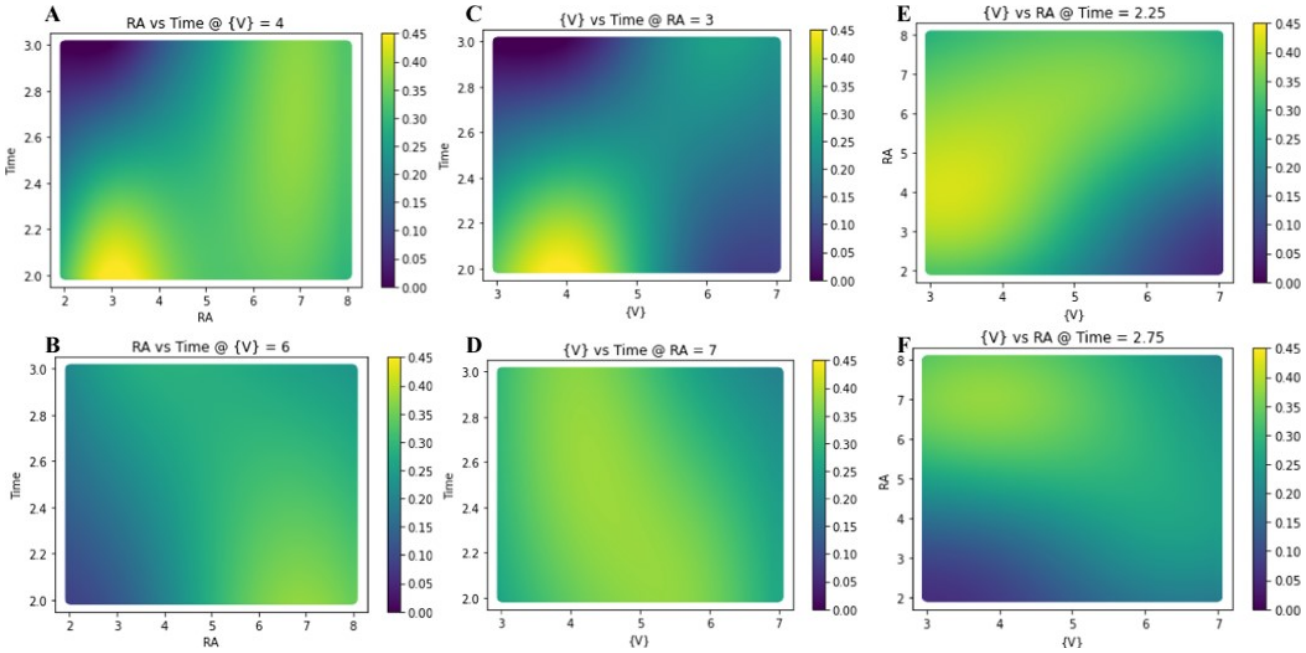

Figure 5. Interpolated heat maps showing slices of the three-dimensional chemical space for the significant factors in Fe-linked $\{V_{18}\}$ network synthesis at the higher (+1) and lower (−1) settings analyzed in these experiments. High yield = yellow; low yield = blue. $\{V\} = V_2O_5$ concentration (mmol), RA = reducing agent concentration (hydrazine sulfate, mmol), and time (h). SI, Section 3.2.4 describes how the plot was prepared.

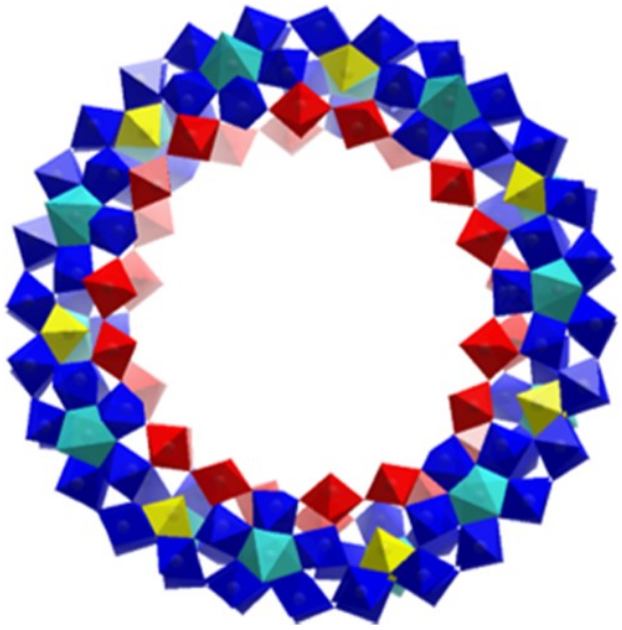

Figure 6. Polyhedral representation of the $\{Mo_{154}\}$ wheel structure shown from a top-down perspective highlighting seven $\{Mo_{11}\}$ units, where $\{Mo_1\}$ = yellow, $\{Mo_2\}$ linker-type = red, and $\{(Mo)Mo_5\}$ pentagonal-type = light blue/blue.

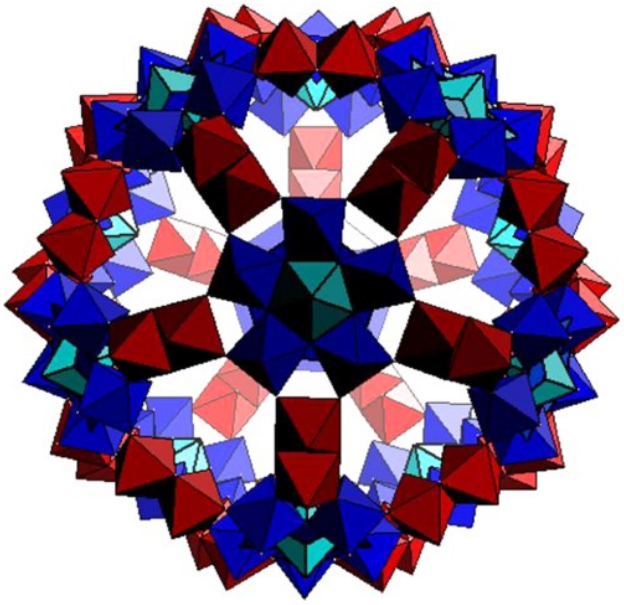

Figure 7. Polyhedral representation of the $\{Mo_{132}\}$ Keplerate structure, where the pentagonal-type $\{(Mo)Mo_5\}$ = light blue/blue and the edge-sharing $\{Mo_2\}$ linker-type = red.

The synthetic procedure for the Keggin-Net reported involves four key reactants and three process steps that were identified as likely to be relevant (three pH adjustments and a stirring period). Thus, the factors chosen to investigate were morpholine, which acts as the cation for crystallization of the product; $\{W_{10}\}$ precursor ($K_8SiW_{10}O_{36}\cdot 12H_2O$) and the heterometallic redox agents $Mn(II)SO_4\cdot H_2O$ and $KMnO_4$, which react together to provide Mn(III) ions for the Keggin-Net. Only one pH adjustment was used as a factor after some preliminary experiments found the adjustment after Mn(II) addition to be the largest. The levels of each of the factors were varied from ca. 80% at the lower level to ca. 120% at the higher setting for each reagent, while pH was varied ±0.15. The temperature was set at 30 or 80 °C to capture the difference between room and elevated temperature.

https://doi.org/10.1021/acs.chemmater.1c01401
Chem. Mater. 2021, 33, 7263−7271

Table 1. Two-Level Settings and Disentangled Factor Effects for the Keggin-Net and the Fe-Linked $\{V_{18}\}$[a]

POM	Keggin-Net				Fe-linked $\{V_{18}\}$			
label	factor	−1	+1	effect[a]	factor	−1	+1	effect[a]
A	NR_3[c]	22.9	34.4	−0.06	LiOH	4.0	6.0	0.6
B	$\{W_{10}\}$	0.10	0.13	0.41	V_2O_5	2.25	2.75	−3.4
C	Mn(II)	0.13	0.20	−1.29	T	60	95	0.2
D	$KMnO_4$	31.6	41.1	0.48	RA[b]	2.0	40	3.5
E	pH	7.60	7.90	0.41	$FeCl_2$	1.0	1.5	1.9
F	T	30.0	80.0	0.55	t	180	420	−3.4

[a]All reagent quantities are in mmol. All temperatures (T) are in °C. All times (t) are in minutes. Keggin-net scale = 55 mL, minimum significant factor effect = 0.53×10^{-2}; Fe-linked $\{V_{18}\}$ scale = 35 mL, minimum significant factor effect = 6.9×10^{-2}. [b]RA = hydrazine sulfate. [c]NR_3 = morpholine.

Three 12-reaction screening experiments were conducted by varying factors A−F as shown in Table 1 at their maximum or minimum setting. In the Keggin network experiments, the minimum significant factor effect was calculated to be 5.3×10^{-3} and the absolute value of any effect had to be equal or higher to be considered as significant. The stoichiometry of manganese sulfate ($MnSO_4 \cdot 4H_2O$) and the heating temperature were found to have significant effects on the outcomes, whereas the concentration of potassium permanganate ($KMnO_4$) did not pass the threshold of being significant, but its effect was still considerably high and worth mentioning here. The negative value of the Factor effect indicates that higher yields were achieved with Factor C at the lower setting, demonstrating that the ratio of $MnSO_4 \cdot 4H_2O$ to $\{\gamma\text{-}SiW_{10}\}$ should be closer to 1:1 than 2:1 (or Mn: Si:10 W = 1:1:10) to achieve the optimal conditions for self-assembly of the Keggin network (Mn:Si:W = 12:7:72). Morpholine has the least effect, likely due to the fact that it exists in significant excess (180−350 equiv) in solution at either setting; however, this may also be a result of its role as a counter cation, rather than an integral part of the POM self-assembly process, suggesting that crystallization is not the limiting factor in the synthesis of this POM.

Next, a full factorial design for these three factors was run with the −1 and +1 settings, the same as above (Table 3). This was run to assess the effects of factor interactions calculated from (C × D), (C × F), and (D × F) alongside the effects of the main factors (see Table S2 and the Supporting Information Spreadsheets for full design details). Applying this analysis showed that $MnSO_4$ was the most significant factor followed by $KMnO_4$ likely due to the need to oxidize Mn(II) to Mn(III) in this reaction. The interaction effect for these two factors (CD) was negative meaning that the ideal ratio of Mn(II):Mn(VII) is ≈3:1, which assumes that complete conversion would yield 3 Mn(III) + 1 Mn(IV) center. The effect of reaction temperature individually was also found to be important with the higher setting found to be more favorable.

$\{V_{18}\}$ Fe-Linked Network. The $\{V_{18}\}$ network was first mentioned in 1999[22,23] and is an example of a three-dimensional (b)-type framework displaying a regular cubic arrangement of kegginoid $\{XV_{18}O_{42}\}$ clusters (where X = SO_4 or VO_4) linked together through $Fe(H_2O)_4$. The high porosity of this scaffold allows the interpenetrations of two slightly shifted frameworks as can be seen in Figure 4. Each POM cluster binds to six transition metal centers $\{Fe(H_2O)_4\}$, which results in the general formula $[Fe_3V_{10}{}^{IV}V_8{}^{V}O_{42}(H_2O)_{12}(XO_4)] \cdot 24H_2O$ (X = V or S). In $\{V_{18}\}$ Fe-linked network experiments (Table 1), the minimum significant factor effect was calculated as 6.9×10^{-2}, but unfortunately, none of the effects were found to meet this threshold. However, three factors had far higher effects than the others: (1) the concentration of vanadium pentoxide (V_2O_5), (2) the concentration of hydrazine sulfate ($[N_2H_5][HSO_4]$), and (3) the reaction time. Surprisingly, the reaction temperature did not play an important role in the synthesis, whereas a higher yield was achieved when the reaction time was shorter and the concentration of vanadium pentoxide (V_2O_5) was lower. The ratio of hydrazine sulfate to vanadium pentoxide seemed to be maximal around 2:1, providing an excess of both reducing electrons and sulfate anions and thus suggesting V reduction may be a key mechanistic step in the formation of this cluster. However, reactions with separate sulfate sources may be required to disentangle these two possibilities.

Upon running a full factorial design, the significance of the reducing agent is still clear with this providing the most important factor (Table 3) with the other factors and factor interactions yielding only small and likely statistically insignificant effects. Statistical analysis of the data collected for the V_{18} synthesis suggests low R^2 values for the derived model, suggesting that further runs would be required to gain more certainty in the key factor effects.

Interpolated 2D heat maps can be generated from the DOE data, which provides a way to visualize the results graphically (Figure 5). The interacting effect of time (F) and reducing agent (D) can be seen by plotting them at a low [V] setting (top left). This shows that the positive effect of reducing agent on yield at short times falls away rapidly upon increasing stir time at low reducing agent concentration but less so when the reducing agent is high. This may be due to aerobic oxidation over time limiting the amount of reducing electrons available for the POM synthesis. At high reducing agent concentration, the chemical space is relatively flat showing good yields at most vanadium concentrations particularly for shorter reaction times (bottom center). This reflects the smaller effect significance of the vanadium concentration.

Finally, by controlling for reaction times, the more marginal effect of the vanadium can be visualized (bottom right) with higher yields at lower values reflecting the negative value of the factor effect. Intriguingly, the data appears to show an "island" of high yield at low reducing agent concentration when reaction times are short and vanadium concentration is low, suggesting these two factors combined may be able to overcome the disadvantageous effect of the lower reducing agent concentration; however, the DOE analysis suggests that this does not in fact represent the true optimum and the idealized synthesis will include reducing agent at its higher setting while both the vanadium and time should be at their lower values.

https://doi.org/10.1021/acs.chemmater.1c01401
Chem. Mater. 2021, 33, 7263−7271

Table 2. Two Level Settings and Disentangled Factor Effects for $\{Mo_{154}\}$ and $\{Mo_{132}\}$.[a]

POM	$\{Mo_{154}\}$				$\{Mo_{132}\}$					
label	factor	−1	+1	effect[b]	factor	−1	+1	effect[b]	xtal	comb.
A	Na_2MoO_4	0.83	2.07	7.0	OAc[c]	10.0	16.2	10.0	3.5	13.5
B	RA[c]	0.23	0.77	6.2	$\{Mo_7\}$	0.40	0.49	1.2	1.9	0.7
C	pH	0.8	1.2	−5.5	pH	3.80	4.20	0.6	4.1	4.8
D	*T*	20	60	−1.9	RA[c]	0.54	0.69	0.8	0	0.8
E	*t*	10	60	−2.3	*T*	20	60	−1.6	3.7	−2.0
F	evap.	slow	fast	−0.1	*t*	10	60	−2.5	3.0	0.4

[a]All reagent quantities are in mmol. All temperatures (*T*) are in °C. All times (*t*) in minutes. $\{Mo_{132}\}$ Scale = 47 mL, Minimum Significant Factor Effect for precipitate (ppt) , single crystals (xtal) and combined (Comb.) = 4.2×10^{-2}, 1.8×10^{-2} and 3.7×10^{-2}. All times (t) in minutes. $\{Mo_{154}\}$ scale = 27.1 mL, minimum significant factor effect = 6.5×10^{-2}; $\{Mo_{132}\}$ scale. [b]$\times 10^{-2}$. [c]RA = hydrazine sulfate. [d]NR_3 = morpholine.

Table 3. Full Factorial Main and Two-Factor Interaction Effects for the Three Most Influential Factors Studied in the Screening Experiments (Above) in Order of Absolute Effect[a]

Keggin-net	R^2 = 0.97		Fe-linked $\{V_{18}\}$	R^2 = 0.32		Mo_{154}	R^2 = 0.97	Mo_{132}	R^2 = 0.90	
factor	effect[d]	*p*	factor	effect[d]	*p*	factor	effect[b]	factor	effect[d]	*p*
$MnSO_4$ (C)	−13.16	0.005	RA[c] (D)	12.46	0.217	Na_2MoO_4 (A)	60.7	NH_4OAc (A)	22.8	0.017
$KMnO_4$ (D)	4.64	0.010	BF	−1.88	0.364	AB	44.6	AC	−4.93	0.081
temp. (F)	4.11	0.011	*t* (F)	−0.75	0.225	RA[c] (B)	38.6	pH (C)	3.00	0.037
CD	−2.72	0.010	V_2O_5 (B)	0.56	0.451	BC	19.0	AE	−0.73	0.174
CF	1.74	0.068	DF	0.46	0.611	pH (C)	−14.9	temp. (E)	0.46	0.171
DF	−0.36	0.244	BD	0.34	0.388	AC	−0.43	CE	−0.42	0.965

[a]All reagent quantities in mmol. All temperatures (T) in °C. All times (t) in minutes. $\{Mo_{132}\}$ Scale = 47 mL, Minimum Significant Factor Effect for precipitate (ppt) , single crystals (xtal) and combined (Comb.) = 4.2×10^{-2}, 1.8×10^{-2} and 3.7×10^{-2}. [b]$\times 10^{-2}$. [c]RA = hydrazine sulfate. [d]$[NH_4]$ salt.

$\{Mo_{154}\}$ Blue Wheel. Molybdenum blues are without a doubt widely accepted as remarkable examples of polyoxoanion self-assembly, especially considering the simplicity of their synthetic procedures. They are defined by containing mixed-valence Mo^V/Mo^{VI} addenda having delocalized electrons capable of intervalence charge transfer from Mo^{VI} to Mo^V, and it is this electronic interaction that gives the clusters their signature intense blue color. The self-assembly of molybdenum blues occurs in aqueous Mo^{VI} solutions by the interaction of reducing agents and acids. We have recently demonstrated that the mechanism of Mo_{154} formation occurs through an autocatalytic process, whereby the rate of reductive dimerization of molybdate to the Mo_2 building block is key to the isolation of the wheel structure over other topologies (e.g., Keplerate Mo_{132}). As such we hypothesized that the concentration of reducing agent would be a key factor in this synthesis, as well as potential pH and MoO_4 concentration, since reduction potential is closely related to metal oxide protonation.

In the $\{Mo_{154}\}$ blue wheel experiment (Table 2), the minimum significant factor effect, for the initially collected precipitate from the reaction, was calculated to be 6.5×10^{-2}. The stoichiometry of both molybdate and hydrazine sulfate ($[N_2H_5][HSO_4]$) were found to have a significant effect on the outcome, whereas the pH did not pass the threshold of being significant but was still considerably high.

The positive value of Factor effect A suggests that concentration is important for this reaction; however, the negligible effect of evaporation for crystallization may indicate this is less related to the formation of crystals than other factors related to a concentration such as the rate of aerobic oxidation. This would be in keeping with the observation that the reducing agent hydrazine sulfate ($[N_2H_5][HSO_4]$) was the second most important factor and produced greater yields when at the higher setting. The preference for a lower pH setting also validates our mechanistic studies which showed that Mo_{154} dominated over Mo_{132} at lower pH, presumably due to more facile reduction when metal oxide ligands are protonated.

After the application to a full factorial design (Table 3), the molybdate concentration was still found to be the most important effect followed by the reducing agent. However, the interaction effect of these two was found to be larger than the reducing agent alone, demonstrating that the formation of reduced Mo(V) is key to the mechanism of Mo_{154} formation. Interestingly, no significant interaction was found for molybdate concentration and pH. Instead, the interaction of reducing agent with pH (positive) was found to be the next most important factor, higher even than pH alone reflecting the more facile reduction with lower pH (−1 setting) and higher reductant concentration (+1 setting). These data may indicate that Mo_{154} formation is more thermodynamically controlled than the $\{V_{18}\}$ synthesis.

$\{Mo_{132}\}$ Brown Keplerate. In principle, molybdenum browns are further reduced relative to molybdenum blues and, rather than being delocalized throughout the entire molecule, additional electrons that are found in this species are localized between reduced Mo^V centers in Mo−Mo bonds contributing to the brown color of these clusters, see Figure 7. That means, when the pH is slightly increased, the self-assembly tends toward the formation of remarkable spherical anions colloquially referred to as Keplerate clusters due to Johannes Kepler's early model of the cosmos.[24] The $\{Mo_{132}\}$ spherical structure can also be described as 12 $\{Mo_{11}\}$ units which, however, are different to the ones found in $\{Mo_{154}\}$. The central $\{(Mo)Mo_5\}$ building blocks are linked together by five $\{Mo_2\}$ linker-type units connected via edge-sharing among themselves leading to a smaller, fully spherical, icosahedral

https://doi.org/10.1021/acs.chemmater.1c01401
Chem. Mater. 2021, 33, 7263−7271

topology.[25−28] This structure has an internal cavity size with a diameter of 17 Å and an outer diameter of 25 Å. The building block approach to the formation of the Keplerate structures leaves 20 hexagonal open spaces, referred to as pores, on the sphere's surface. This internal cavity of this Keplerate can be used for the study of guest−host chemistry.

In $\{Mo_{132}\}$ Keplerate experiments (Table 2), the minimum significant factor effect was calculated to be 4.2×10^{-2}, although none of the effects were found to be significant enough in this initial analysis. Despite this, the pH adjustment by 50% acetic acid (CH_3COOH) almost passed the threshold. The effects of following the reaction temperature and the concentration of ammonium acetate (CH_3COONH_4) were rather close to the minimum significant factor effect and high enough to be noteworthy. The positive value of the Factor effect indicates that higher yields were achieved with Factor C at the higher setting, demonstrating that the pH should be higher to achieve the optimal conditions for the self-assembly of $\{Mo_{132}\}$ Keplerate. Interestingly, hydrazine sulfate ($[N_2H_5]$-$[HSO_4]$) has the least effect here, which might be lead back to the small difference between the two settings or the predominant influence of the pH.

Two weeks after the removal and collection of the dark brown $\{Mo_{132}\}$ Keplerate solid material, large dark brown crystals had formed. They were analyzed in the same manner as the other POM products from all of the other reactions.In the $\{Mo_{132}\}$ Keplerate crystal analysis, the minimum significant factor effect was calculated to be 1.8×10^{-2} (Table 2). The stoichiometry of ammonium acetate (CH_3COONH_4) and the reaction time were found to have significant effects, whereas the reaction temperature almost passed the threshold of being significant. The outstanding positive effect of factor A indicates that a higher concentration of ammonium acetate (CH_3COONH_4) leads to higher yields. This could be easily identified because only the samples with the higher setting of factor A formed crystals, whereas the others had no yields at all. Surprisingly, a shorter reaction time yielded better results, while the opposite was the case in the previous results. This makes sense though because less material reacted and was collected as precipitate.

Keplerate $\{Mo_{132}\}$ Combined Results. Interestingly, the results for $\{Mo_{132}\}$ Keplerate precipitate and crystals were not equivalent. The concentration of ammonium acetate (CH_3COONH_4) and the reaction temperature were among the three most important factors in both cases, only the pH adjustment by 50% acetic acid (CH_3COOH) and the reaction time differed in the results. Removing the precipitate after a few days could also be examined as a factor because crystals formed afterwards in only the six flasks containing the higher concentration of ammonium acetate (CH_3COONH_4).

Combining the results of both crops of Mo_{132} allows a clearer picture of the overall effects on the synthesis of Keplerate. The minimum value for significance of the combined results was found to be 3.7×10^{-2} (Table 2). Both ammonium acetate and pH were found to be key, but the subtle effects of temperature and time were not significant in this analysis. After the application to a full factorial design, the most important significant factor was still ammonium acetate by almost an order of magnitude with the higher concentration yielding more desired product (Table 3). pH was the third most important factor with the interaction between these two constituting the second most important factor. Intriguingly, the interaction factor effect was found to be negative, while the main effects were both positive meaning that a high pH (achieved through the addition of HOAc) is able to compensate somewhat for a lower concentration of ammonium acetate, while if both are low, then formation of the product is decimated. Thus, the effect of NH_4OAc may be a result of the pH buffering effect of acetate than the crystal packing provided by the ammonium cation. Future experiments with a range of acetate salts would be expected to confirm this hypothesis.

Optimized Syntheses. For all of the four families discussed, optimized syntheses were designed based on the results of the DOE analysis (see the SI). Where a factor clearly influenced the yield, it was set at its more favorable setting; however, if the factor showed little to no impact on yield, this value was set either at the midpoint value or at the setting which placed the least additional burden on the synthetic protocol (i.e., if the temperature had no effect, this was set at room temperature). The improvements in the synthesis unveiled by our DOE analysis gave on average a 33% increase in yield over the top yields reported in the literature. For Fe-linked V_{18}, almost no increase from the literature value (57% vs lit. 56%) was observed under the optimal conditions; however, the yield was higher than almost all of our other iterations of this synthesis. The Keggin-Net synthesis was increased to a 28% yield, higher than the 22% reported in the literature and significantly higher than the highest in our screening experiments of 11%. The Mo_{154} synthesis yield increased from 45 to 60% after our investigations and the Mo_{132} from 52 to 71%, demonstrating the utility of the DOE method for optimizing inorganic syntheses.

■ CONCLUSIONS

In three of the four POM syntheses, the redox modulating reagent was found to be one of the most significant factors affecting yield, demonstrating the vital importance of electron transfer processes in the formation of these complex nanostructures. Given this it is interesting to note that most POM syntheses are carried out under aerobic conditions, where the oxidation rate at the solution surface is not well controlled. Curiously, the only POM which did not feature reducing agent as a key factor is the most reduced POM $\{Mo_{132}\}$ containing 30 Mo(V) dimer units per cluster; however, this is most likely a result of the large (ca. 10 fold) excess of the reducing agent wrt Mo under our DOE conditions. For Mo_{132}, ammonium acetate was the most significant by a large degree followed by the pH, which under our conditions was modulated by the addition of acetic acid. The full factorial analysis demonstrated an interaction effect between these two such that high pH was able to mitigate a lower concentration of ammonium acetate, suggesting some buffering role for the acetate base being key to increased yield as opposed to the facilitation of crystallization by the ammonium cation, which is commonly posited.

Overall, we have provided a standard methodology for the use of DOE in inorganic synthesis by varying six factors ca. ±10−20% from their reported values. We have further demonstrated that by applying a full factorial analysis on the three most significant factors we can elucidate factor interactions that provide key insights into the chemical basis for improved yields. We have produced a simple template for the design of experiments planning (SI, Spreadsheet), which produces a machine-readable csv file for the automated optimization reaction. In the case of notoriously unpredictable POM formations and syntheses, it provided guidance as to

https://doi.org/10.1021/acs.chemmater.1c01401
Chem. Mater. 2021, 33, 7263−7271

which variables are the most important allowing for procedure optimization and targeted troubleshooting of failed syntheses. We have thus written optimized procedures for these POMs, which have provided up to a 73% increase in yield over those reported previously. In addition, the lessons learned from these specific POMs regarding the importance of redox agents and pH buffers can be extrapolated to the whole wealth of POM syntheses providing opportunities to improve yields and our understanding of their self-assembly across the field.

■ ASSOCIATED CONTENT

Supporting Information

The Supporting Information is available free of charge at https://pubs.acs.org/doi/10.1021/acs.chemmater.1c01401.

Full calculations and the template for DOE design (XLSX)

Detailed synthetic procedures, tables of yields, DOE designs, and optimized procedures (PDF)

■ AUTHOR INFORMATION

Corresponding Author

Leroy Cronin − *School of Chemistry, University of Glasgow, Glasgow G12 8QQ, U.K.;* orcid.org/0000-0001-8035-5757; Email: Lee.Cronin@Glasgow.ac.uk

Authors

Nicola L. Bell − *School of Chemistry, University of Glasgow, Glasgow G12 8QQ, U.K.;* orcid.org/0000-0002-7497-9667

Manuel Kupper − *School of Chemistry, University of Glasgow, Glasgow G12 8QQ, U.K.*

Complete contact information is available at: https://pubs.acs.org/10.1021/acs.chemmater.1c01401

Author Contributions

†N.L.B. and M.K. contributed equally to this work.

Notes

The authors declare no competing financial interest.

■ ACKNOWLEDGMENTS

This work was supported by the EPSRC grants (No. EP/J015156/1, EP/L023652/1, EP/I033459/1, EP/J015156/1, EP/K023004/1, EP/L023652/1) and the ERC for an Advanced grant (ERC-ADG, 670467 SMART-POM). The authors would like to thank Jim Mclver for TGA and ICP measurements, Yibin Jiang for help with code for Figure 5, and Eduardo Garrido-Ribo for help with figures.

■ REFERENCES

(1) Lendrem, D. W.; Lendrem, B. C.; Rowland-Jones, R.; D'Agostino, F.; Linsley, M.; Owen, M. R.; Isaacs, J. D. Teaching examples for the design of experiments: geographical sensitivity and the self-fulfilling prophecy. *Pharm. Stat.* **2016**, *15*, 90−92.

(2) Lendrem, D. W.; Lendrem, B. C.; Woods, D.; Rowland-Jones, R.; Burke, M.; Chatfield, M.; Isaacs, J. D.; Owen, M. R. Lost in space: design of experiments and scientific exploration in a Hogarth Universe. *Drug Discovery Today* **2015**, *20*, 1365−1371.

(3) Durakovic, B. Design of Experiments Application, Concepts, Examples: State of the Art. *Period. Eng. Nat. Sci.* **2017**, *5*, 421−439.

(4) Lazic, Z. R. *Design of Experiments in Chemical Engineering: A Practical Guide*; Wiley, 2004; pp 1−620.

(5) Paulo, F.; Santos, L. Design of experiments for microencapsulation applications: A Review. *Mater. Sci. Eng., C* **2017**, *77*, 1327−1340.

(6) Weissman, S. A.; Anderson, N. G. Design of Experiments (DOE) and Process Optimization. A Review of Recent Publications. *Org. Process Res. Dev.* **2015**, *19*, 1605−1633.

(7) Yu, P.; Low, M. Y.; Zhou, W. Design of experiments and regression modelling in food flavour and sensory analysis: A review. *Trends Food Sci. Technol.* **2018**, *71*, 202−215.

(8) Bell, G. H.; Ledolter, J.; Swersey, A. J. A Plackett-Burman Experiment to Increase Supermarket Sales of a National Magazine. *Interfaces* **2009**, *39*, 145−158.

(9) Cao, B.; Adutwum, L. A.; Oliynyk, A. O.; Luber, E. J.; Olsen, B. C.; Mar, A.; Buriak, J. M. How To Optimize Materials and Devices via Design of Experiments and Machine Learning: Demonstration Using Organic Photovoltaics. *ACS Nano* **2018**, *12*, 7434−7444.

(10) Hibbert, D. B. Experimental design in chromatography: A tutorial review. *J. Chromatogr. B* **2012**, *910*, 2−13.

(11) Garud, S. S.; Karimi, I. A.; Kraft, M. Design of computer experiments: A review. *Comput. Chem. Eng.* **2017**, *106*, 71−95.

(12) Gilman, J.; Walls, L.; Bandiera, L.; Menolascina, F. Statistical Design of Experiments for Synthetic Biology. *ACS Synth. Biol.* **2021**, *10*, 1−18.

(13) Castillo, P.; Magnin, J.-P.; Velasquez, M.; Willison, J. Modeling And Optimization of Hydrogen Production By The Photosynthetic Bacterium Rhodobacter capsulatus By The Methodology Of Design Of Experiments (DOE): Interaction Between Lactate Concentration And Light Luminosity. *Energy Procedia* **2012**, *29*, 357−366.

(14) Das, A. K.; Dewanjee, S. Chapter 3 - Optimization of Extraction Using Mathematical Models and Computation. In *Computational Phytochemistry*; Sarker, S. D.; Nahar, L., Eds.; Elsevier, 2018; pp 75−106.

(15) Vander Heyden, Y.; Nijhuis, A.; Smeyers-Verbeke, J.; Vandeginste, B. G. M.; Massart, D. L. Guidance for robustness/ruggedness tests in method validation. *J. Pharm. Biomed. Anal.* **2001**, *24*, 723−753.

(16) Sécheresse, F. *Polyoxometalate Chemistry Some Recent Trends*; World Scientific, 2013; pp 1−305.

(17) Miras, H. N.; Mathis, C.; Xuan, W.; Long, D.-L.; Pow, R.; Cronin, L. Spontaneous formation of autocatalytic sets with self-replicating inorganic metal oxide clusters. *Proc. Natl. Acad. Sci. U.S.A.* **2020**, *117*, 10699−10705.

(18) Stanbury, P. F.; Whitaker, A.; Hall, S. J. *Principles of Fermentation Technology*; Butterworth Heinemann, 1984; pp 1−351.

(19) Stowe, R. A.; Mayer, R. P. Efficient screening of process variables. *Ind. Eng. Chem.* **1966**, *58*, 36−40.

(20) Box, G. E. P.; Meyer, R. D. An Analysis for Unreplicated Fractional Factorials. *Technometrics* **1986**, *28*, 11−18.

(21) Ritchie, C.; Streb, C.; Thiel, J.; Mitchell, S. G.; Miras, H. N.; Long, D.-L.; Boyd, T.; Peacock, R. D.; McGlone, T.; Cronin, L. Reversible Redox Reactions in an Extended Polyoxometalate Framework Solid. *Angew. Chem., Int. Ed.* **2008**, *47*, 6881−6884.

(22) Khan, M.; Yohannes, E.; Doedens, R. M3V18O42(H2O)12(XO4)]·24 H2O (M = Fe, Co; X = V, S): Metal Oxide Based Framework Materials Composed of Polyoxovanadate Clusters. *Angew. Chem., Int. Ed.* **1999**, *38*, 1292−1294.

(23) Miras, H. N.; Mathis, C.; Xuan, W.; Long, D.-L.; Pow, R.; Cronin, L. Spontaneous formation of autocatalytic sets with self-replicating inorganic metal oxide clusters. *Proc. Natl. Acad. Sci. U.S.A.* **2020**, *117*, 10699−10705.

(24) Müller, A.; Krickemeyer, E.; Bögge, H.; Schmidtmann, M.; Peters, F. Organizational Forms of Matter: An Inorganic Super Fullerene and Keplerate Based on Molybdenum Oxide. *Angew. Chem., Int. Ed.* **1998**, *37*, 3359−3363.

(25) Müller, A.; Sarkar, S.; Shah, S. Q. N.; Bögge, H.; Schmidtmann, M.; Sarkar, S.; Kögerler, P.; Hauptfleisch, B.; Trautwein, A. X.; Schünemann, V. Archimedean Synthesis and Magic Numbers: "Sizing" Giant Molybdenum-Oxide-Based Molecular Spheres of the Keplerate Type. *Angew. Chem., Int. Ed.* **1999**, *38*, 3238−3241.

(26) Müller, A.; Todea, A. M.; van Slageren, J.; Dressel, M.; Bögge, H.; Schmidtmann, M.; Luban, M.; Engelhardt, L.; Rusu, M. Triangular Geometrical and Magnetic Motifs Uniquely Linked on a

Spherical Capsule Surface. *Angew. Chem., Int. Ed.* **2005**, *44*, 3857−3861.
(27) Müller, A.; Bögge, H.; Sousa, F. L.; Schmidtmann, M.; Kurth, D. G.; Volkmer, D.; van Slageren, J.; Dressel, M.; Kistler, M. L.; Liu, T. Nanometer-Sized Molybdenum−Iron Oxide Capsule-Surface Modifications: External and Internal. *Small* **2007**, *3*, 986−992.
(28) Todea, A. M.; Merca, A.; Bögge, H.; van Slageren, J.; Dressel, M.; Engelhardt, L.; Luban, M.; Glaser, T.; Henry, M.; Müller, A. Extending the {(Mo)Mo5}12M30 Capsule Keplerate Sequence: A {Cr30} Cluster of S=3/2 Metal Centers with a {Na(H2O)12} Encapsulate. *Angew. Chem., Int. Ed.* **2007**, *46*, 6106−6110.

https://doi.org/10.1021/acs.chemmater.1c01401
Chem. Mater. 2021, 33, 7263−7271